THE ASTROPHYSICAL JOURNAL, 338:244–261, 1989 March 1

THE ORION-KL SUPER WATER MASER

GUIDO GARAY,[1,2,3] J. M. MORAN,[1] AND A. D. HASCHICK[1,4]
Received 1988 May 9; accepted 1988 August 9

ABSTRACT

For 7 years we monitored the polarization characteristics of the most powerful water maser feature ever seen in the Orion molecular cloud. The maser radiation was highly (~60%) linearly polarized and the degree of polarization generally decreased as the flux density increased. The polarization parameters suggest that the maser cloud was embedded in a magnetic field with a strength of ~30 mG. We inferred that the magnetic field direction made an angle of ~30° to the line of sight, and its projection in the plane of the sky was along a position angle of roughly −15°.

A plot of the flux density versus time shows several outbursts, which reached values as large as $\sim 6.7 \times 10^6$ Jy, superposed on a "quiescent" level of $\sim 0.5 \times 10^6$ Jy. Since early 1986, the maser feature has been comparatively weak, and by mid 1987, its flux density had dropped to 0.7×10^5 Jy. On the assumption of isotropic emission, the peak luminosity in the water maser line was 0.02 $L_\odot$, equivalent to a photon emission rate of 6×10^{47} s^{-1}. The energy radiated over its lifetime was 6×10^{39} ergs. During one of the outbursts—not the most luminous one—the brightness temperature reached 3×10^{15} K, implying that the maser was probably saturated. The line width and center velocity of the maser varied with time, most likely due to blending of two or more features that varied in strength. The kinetic temperature of the gas, derived from the maser line width, was ~150 K.

The observed flux densities at infrared wavelengths of sources in the vicinity of the Orion-KL region suggest that the super maser was unlikely to have been radiatively pumped, either by an internal or by an external energy source. The maser may have been excited by a magnetohydrodynamic shock wave propagating into a dense, magnetized, fragment of gas embedded in the Orion molecular cloud. Such a maser could have been collisionally pumped in regions where the electron temperature was much higher than that of the neutral particles.

Subject headings: interstellar: magnetic fields — interstellar: molecules — masers — nebulae: Orion Nebula — polarization — radio sources: variable

I. INTRODUCTION

The spectra of the water vapor maser emission toward the Orion Kleinmann-Low (KL) nebula show strong, low-velocity lines with velocities in a range of ±20 km s^{-1} about the radial velocity of the molecular cloud of 8 km s^{-1} and weak, high-velocity lines spanning a velocity range of ±100 km s^{-1} around the low-velocity features (Sullivan 1973; Moran *et al.* 1977; Genzel and Downes 1977). Proper-motion measurement of the individual maser components showed that the low- and high-velocity features are expanding away from a common central point, probably the infrared source IRc2 (Genzel *et al.* 1981).

Abraham, Opher, and Rafaelli (1979) reported a spectacular flare in the water vapor maser emission from the KL nebula, which began in 1979 August. The flare, at a velocity of ~8 km s^{-1}, had a flux density greater, by more than two orders of magnitude, than the previous strongest component. Early observations of this H_2O maser feature, during its initial outburst, were made by Matveenko, Kogan, and Kostenko (1980), who reported large (about one order of magnitude) variations in its flux density on a time scale of 1 day. Interferometric observations in late 1979 provided a measure of the angular size of the flare spot of ~0".001, which implied a brightness temperature of 10^{15} K (Matveenko, Moran, and Genzel 1982). The angular size was also ~0".001 in mid 1982 (Matveenko *et al.* 1983). A more extensive monitoring of the flare feature by Abraham *et al.* (1981, 1986) showed large fluctuations in the flux density on a time scale of several months. The fluctuations are characterized by a rapid increase in the flux density over a few weeks followed by a slow decay to the initial value over several months. An early characterization of the physical properties of the maser was made by Strelnitskii (1982).

The characteristics of the polarization of maser emission provide a powerful probe to diagnose the physical conditions inside the maser cloud (Goldreich, Keeley, and Kwan 1973*a*, *b*; hereafter GKK). If the Zeeman splitting is smaller than the line width of the maser radiation, as is generally the case for the water masers, GKK's theories predict that unsaturated masers should emit unpolarized radiation whereas saturated masers might emit linearly polarized radiation. In particular, if the Zeeman splitting is larger than the stimulated emission rate, then the degree of linear polarization could be large. The study of strong and highly linearly polarized H_2O masers should thus provide information on the strength of the magnetic field in regions of star formation with linear dimensions of ~10 AU and densities of 10^9–10^{11} cm^{-3}. Polarization observations by Abraham *et al.* (1981) showed that the Orion flare feature was highly linearly polarized. We note that linear polarization can also be produced by anisotropic pumping (Western

[1] Harvard-Smithsonian Center for Astrophysics.
[2] University of Chile.
[3] European Southern Observatory.
[4] Haystack Observatory.

and Watson 1983). Circular polarization is expected for the water maser emission only when the Zeeman splitting is large enough to be observed directly (i.e., a 100 mG magnetic field would produce a line splitting of 100 Hz and a peak-to-peak difference of $\sim 1\%$ in the circular polarization spectra). Such a small effect is difficult to detect for maser lines with a high degree of linear polarization in the line because the polarization of the feed horn must be circular to a high precision. In certain cases, but not that of the Orion flare feature, the circular polarization due to the Zeeman effect has been detected (Fiebig and Güsten 1989).

The super water maser in the Orion nebula is the brightest maser ever measured, although masers in W49, and certain extragalactic nuclear masers, may be more luminous. For a flux density of 2×10^6 Jy, a line width of 40 kHz, and a distance of 500 pc, its "isotropic" luminosity is $\sim 0.007\ L_\odot$, and the microwave photon rate is $\sim 2 \times 10^{47}$ photons s^{-1}. Based on the observed narrow line width, Matveenko, Kogan, and Kostenko (1980) concluded that the Orion flare maser emission was unsaturated. However, its high degree of linear polarization and the high brightness temperature strongly suggest that this maser is saturated. The nature of powerful H_2O masers, i.e., those whose photon flux is greater than 10^{46} photons s^{-1}, is poorly understood. Their existence raises serious problems in understanding pump mechanisms and sources of pump energy since the power requirements are so great.

Located in one of the most extensively studied regions of star formation, which has been recently probed with high angular resolution at infrared (Wynn-Williams *et al.* 1984) and radio (Garay, Moran, and Reid 1987) wavelengths, the Orion super water maser provides an ideal case to study the saturation state, the source of excitation, and the physical conditions in strong masers. An observation program was conducted to observe the properties of the super water maser feature in the Orion molecular cloud on a regular basis, in order to understand the physical properties of the strong maser cloud. We report here the behavior of the flux density, velocity, line width, and polarization of the Orion super maser as a function of time from 1980 February to 1987 June. Our measurements are more detailed than those of Abraham, Vilas Boas, and del Ciampo (1986), who did not measure the velocity or line width of the maser. The observations that we made before 1982 July were part of the Ph.D. thesis of Garay (1983).

II. OBSERVATIONS

The monitoring observations of the super maser in Orion were conducted at ~ 1 month intervals from 1980 February to 1987 June using the 37-m parabolic antenna of the Haystack Observatory. The receiver system included a *K* band maser amplifier and a 1024 channel autocorrelator. The system temperatures were in the range of 80–200 K, with the higher temperatures occurring during poor weather conditions. Before 1985 July, the peak aperture efficiency of the antenna (including the radome), which was achieved at 50° elevation, was 21% at 22 GHz, corresponding to a sensitivity to an unpolarized source of 12 Jy K^{-1}. After 1985 July, the radome was replaced, and the efficiency improved to 25%, corresponding to 10 Jy K^{-1}.

The polarization measurements were made with a rotating polarimeter system. The antenna had a circularly polarized feed at the secondary focus with dual orthogonal ports. In front of this feed was mounted a rotatable quarter wave plate (venetian blind type) so that the outputs were orthogonal linear polarizations at position angles determined by the orientation of the quarter wave plate. The observations were conducted in the total power mode with the off-source position offset by $\sim 5°$ in right ascension from the on-source position. The spectra were taken using an 8.3 MHz or a 5.5 MHz total bandwidth, with velocity resolution of 0.13 and 0.09 km s^{-1}, and a total velocity coverage of 112 and 74 km s^{-1}, respectively. The observations were corrected for changes in antenna gain and atmospheric absorption, as a function of elevation angle.

The polarization measurements were calibrated in the following manner. The power $P(\epsilon)$ measured from a linear feed oriented at a position angle ϵ, measured from the north-south direction, is given by

$$P(\epsilon) = \frac{Q}{2}\cos 2\epsilon + \frac{U}{2}\sin 2\epsilon + \frac{I}{2}, \tag{1}$$

where I, Q, U are the Stokes parameters. To determine the Stokes parameters, we made a three-minute on-source spectrum at each of six orientations of the polarimeter, separated by 30° in position angle. Each on-source spectrum was accompanied by its own off-source spectrum. The Stokes parameters I, Q, U could be determined by a least mean square fit of equation (1) to the observations. However, to account for instrumental errors, we modeled the measurements by the equation

$$P(\epsilon) = G(\epsilon)\left\{\frac{Q}{2}\cos 2\epsilon + \frac{U}{2}\sin 2\epsilon + \frac{I}{2}\right\}, \tag{2}$$

where $G(\epsilon)$ is a factor that takes into account variations in atmospheric opacity and antenna pointing, since observations were taken over ~ 40 minutes, and also instrumental gain variations induced by rotating the polarizer. To determine the values of $G(\epsilon)$, we used the low-velocity water maser features contained in the spectra observed toward the Orion-KL region. We first assumed that $G(\epsilon) = 1$ for all ϵ and fitted the data to equation (2) and found that many features were essentially unpolarized. The unpolarized features were then used to compute the function $G(\epsilon)$ by comparing their observed flux densities at the different position angles with their average value of I. Since, for an unpolarized feature, $P(\epsilon) = G(\epsilon)(I/2)$, this procedure permits direct determination of $G(\epsilon)$. The $G(\epsilon)$ factors were computed by analysis of ~ 15 nearly unpolarized features. With this number of features, the effects of small amounts of polarization in various features were minimized. We then proceeded to determine the Stokes parameters by a least mean square fit of the calibrated data [i.e., $P(\epsilon)/G(\epsilon)$] to equation (1). In Figure 1, we show an example of the observed data, calibrated data, and fitted response. The measured values of $G(\epsilon)$ were approximately random with an rms scatter about unity of ~ 0.04.

The polarization angle, τ, and degree of polarization, d, were determined from the Stokes parameters by the relations $\tan 2\tau = Q/U$ and $d = (Q^2 + U^2)^{1/2}/I$. Typical 1 σ formal errors were 1° for the polarization position angle, and 1% for the degree of polarization. On several occasions (see Table 1), we made multiple measurements on a single day and obtained results in agreement to within these errors. An example of the total and polarized power spectrum of the H_2O maser emission toward the Orion nebula taken in 1981 October is shown in Figure 2. Another spectrum of Orion taken in 1987 June is shown in Figure 3.

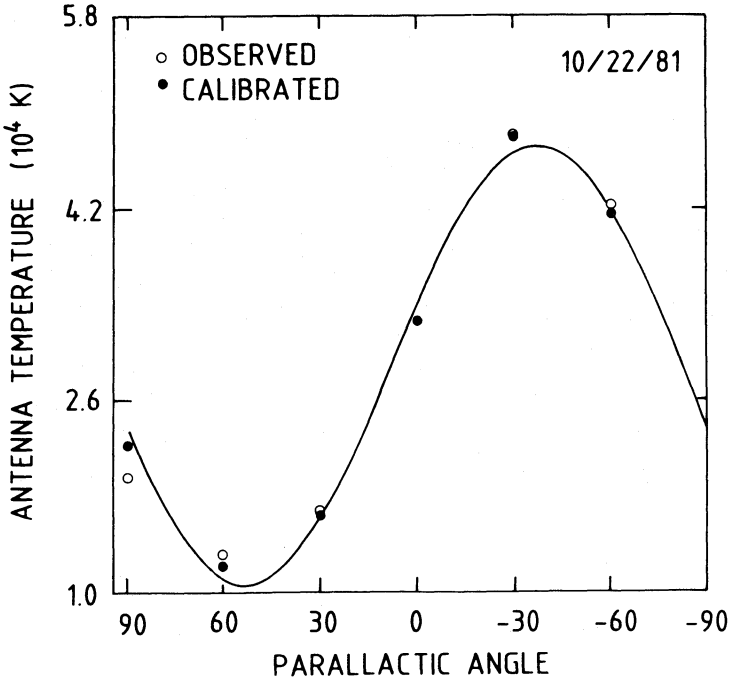

FIG. 1.—Antenna temperature of the Orion super water maser feature plotted as a function of the parallactic angle. *Open dots:* observed values; *black circles:* calibrated values, derived as described in the test. Solid line shows the fit to the calibrated data.

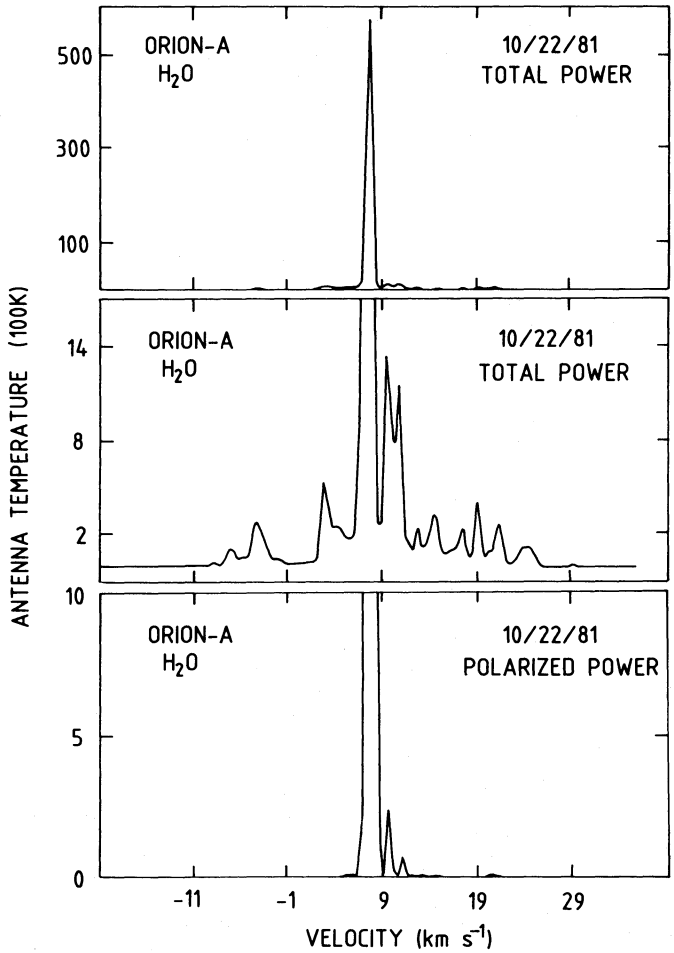

FIG. 2.—*Top:* total power spectrum of the H_2O maser emission toward the Orion-KL region, measured on 1981 October 22, which mostly shows the emission from the flare features at ~ 8.0 km s^{-1}. *Middle:* same as top but clipped, so the weaker H_2O maser features are seen. *Bottom:* power spectrum of the polarized H_2O maser emission. The velocity is referred to the local standard of rest and a rest frequency of 22235.08 MHz.

TABLE 1

OBSERVED PARAMETERS OF THE ORION SUPER H_2O MASER

Date	Day Number	Flux[a] Density (10^6 Jy)	Center Velocity (km s^{-1})	Line Width (km s^{-1})	Position Angle	Degree Polarization %
1980 Feb 13	44	0.62	7.83	0.55	−17.9	52.3
1980 Mar 29	89	1.59	7.70	0.62	−23.1	48.1
1980 Mar 31	91	1.61	7.70	0.62	−21.2	47.5
1980 Apr 22	113	2.03	7.66	0.64	−16.9	44.9
1980 Apr 23	114	2.00	7.66	0.64	−17.8	44.5
1980 Apr 25	116	2.12	7.66	0.64	−18.1	43.9
1980 Jul 16[b]	198	...	7.58	0.58	...	...
1980 Sep 5[b]	249	...	7.59	0.64	...	...
1980 Sep 10	254	0.95	7.59	0.63	−24.3	57.9
1980 Oct 15	289	0.75	7.61	0.67	−24.1	58.8
1980 Oct 16	290	0.73	7.61	0.67	−24.2	59.8
1980 Nov 3	308	0.81	7.61	0.67	−25.0	59.8
1981 Jan 25	391	0.51	7.56	0.71	−29.6	60.4
1981 Feb 14	411	0.53	7.55	0.70	−30.4	61.0
1981 Mar 16	441	0.57	7.50	0.70	−31.5	61.4
1981 Apr 24	480	0.58	7.53	0.70	−31.5	62.4
1981 May 23a	509	0.55	7.53	0.71	−33.3	63.5
1981 May 23b	509	0.54	7.53	0.71	−33.2	62.8
1981 Jul 18	565	0.60	7.49	0.71	−37.3	66.5
1981 Jul 19	566	0.58	7.49	0.71	−37.5	66.3
1981 Aug 28[b]	606	...	7.49	0.72	...	...
1981 Sep 21	630	0.41	7.50	0.72	−36.4	64.0
1981 Sep 22	631	0.40	7.50	0.73	−36.1	63.9
1981 Oct 22	661	0.39	7.55	0.72	−36.8	63.6
1981 Nov 13	683	0.41	7.57	0.70	−36.1	6.29
1981 Nov 14	684	0.41	7.57	0.70	−36.0	63.0
1981 Dec 22	722	0.39	7.57	0.68	−32.7	73.2
1982 Jan 4	735	0.40	7.57	0.68	−37.8	65.0
1982 Feb 24	786	0.45	7.58	0.66	−33.3	63.8
1982 Mar 4[b]	794	...	7.58	0.63	...	...
1982 May 2	853	0.63	7.55	0.60	−29.2	65.0
1982 Jun 1	883	0.64	7.54	0.61	−28.7	61.4
1982 Jul 6a	918	0.69	7.55	0.60	−28.2	62.5
1982 Jul 6b	918	0.69	7.55	0.60	−28.8	61.7
1982 Sep 21	995	1.02	7.50	0.58	−25.8	58.4
1982 Oct 25a	1029	1.18	7.48	0.58	−24.0	57.5
1982 Oct 25b	1029	1.18	7.48	0.58	−24.0	56.9
1982 Nov 25a	1060	1.30	7.47	0.57	−24.5	57.1
1982 Nov 25b	1060	1.27	7.47	0.57	−25.2	57.7
1982 Dec 24	1089	1.25	7.46	0.58	−26.9	56.8
1983 Jan 7a	1103	1.12	7.46	0.58	−25.9	52.2
1983 Jan 7b	1103	1.10	7.46	0.58	−25.7	52.4
1983 Jan 7c	1103	1.11	7.46	0.58	−25.1	50.3
1983 Jan 30a	1126	1.12	7.46	0.58	−24.8	56.8
1983 Jan 30b	1126	1.13	7.46	0.58	−25.5	56.0
1983 Feb 14	1141	1.12	7.46	0.59	−23.8	56.1
1983 Apr 18	1204	1.04	7.49	0.62	...	...
1983 May 2	1218	1.10	7.50	0.64	...	...
1983 May 18a	1234	1.25	7.51	0.63	−22.3	53.9
1983 May 18b	1234	1.20	7.51	0.63	−22.7	54.7
1983 Jun 23	1270	1.51	7.52	0.63	−19.2	52.0
1983 Aug 16	1324	2.99	7.50	0.60	−19.2	51.9
1983 Oct 20	1389	4.37	7.43	0.73	−18.8	52.1
1984 Apr 21	1573	4.09	7.67	0.64	−16.0	51.3
1984 Aug 17	1691	3.46	7.71	0.63	−17.6	56.1
1984 Sep 1a	1706	3.78	7.72	0.63	−16.0	57.9
1984 Sep 1b	1706	3.78	7.72	0.63	−16.1	58.2
1984 Oct 24	1759	6.60	7.67	0.61	−14.6	54.7
1984 Oct 26	1761	6.70	7.66	0.60	−12.7	49.9
1984 Nov 28	1794	6.55	7.66	0.63	−15.6	55.1
1985 Jan 15	1842	6.65	7.62	0.60	−17.0	49.7
1985 Feb 4	1862	6.35	7.60	0.58	−15.2	49.9
1985 Feb 16	1874	5.85	7.59	0.59	−15.2	50.4
1985 Mar 8	1894	4.08	7.58	0.62	−14.9	48.8
1985 Mar 17	1903	3.25	7.57	0.64	−14.4	46.7
1985 Apr 3	1920	2.93	7.57	0.65	−16.4	45.0
1985 Jul 28	2036	2.21	7.59	0.71	−15.7	45.9
1985 Aug 20	2059	1.93	7.61	0.68	−15.0	49.9
1985 Sep 23	2093	1.91	7.68	0.67	−14.3	53.0
1985 Sep 30	2100	1.93	7.69	0.67	−13.7	52.1
1985 Nov 4	2135	2.48	7.77	0.59	−12.0	50.1

[a] Flux density corrected as described in text.
[b] Only one linearly polarized spectrum.

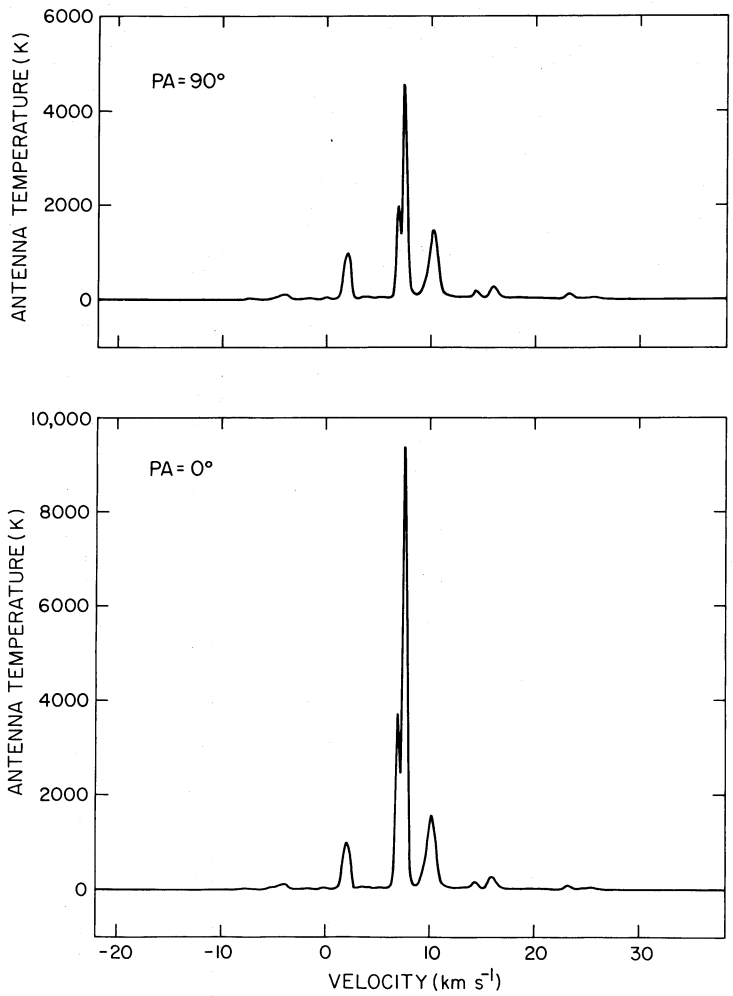

FIG. 3.—*Top:* the water vapor spectrum of the Orion-KL region measured in linear polarization (P.A. 90°) measured on 1987 June 3. The super maser has two distinct components, one at 7.5 and the other at 6.9 km s^{-1}. *Bottom:* spectrum measured at a position angle of 0°. Note that only the super maser is highly polarized. There are many features below 100 K between −10 and 30 km s^{-1} that cannot be seen because of the plot scale.

The center velocity and line width of the super feature were determined by simultaneously fitting a Gaussian profile and a linear baseline to the observed spectra. The velocity resolution used was 0.13 km s^{-1} from 1980 February to 1981 February and 0.09 km s^{-1} from 1981 March through 1987 June. Typical 1 σ formal errors were 0.005 km s^{-1} for the line width, 0.003 km s^{-1} for the center velocity.

The observed flux density of the Orion super feature was corrected for long-term variations in atmospheric opacity and pointing errors in the following way. First, the antenna temperatures of each water maser feature in the spectra were plotted as a function of time. Many features showed random flux variations of less than 10% over time scales of a year or greater. (Occasionally, all features showed correlated changes in their flux densities by $\sim$30%, usually during poor weather conditions.) Subsequently, for calibration purposes, the data set was divided into four periods, of $\sim$15 months each. The "nonvariable" features in a period were then used to compute a flux density scale correction factor for each epoch in that period by comparing their observed flux density in a given epoch with the average flux density over the period. The scale factor of each epoch was computed by a least mean square fit using all (usually $\sim$12) of the "nonvariable" features. This procedure was applied to all four periods, each time using a slightly different set of "nonvariable" features. The scale factors varied from unity by $\pm$6%. The calibration method provides only a relative scale for the flux density; however, the 1 σ errors for this relative flux density are less than 2%. The absolute flux density scale is probably accurate to 10%.

III. RESULTS

a) Long-Term Flux Density Variations

Table 1 presents the observed and derived parameters of the super maser over the first 6 years of the observing period. Table 2 shows the maser parameters during 1986 and 1987 when it consisted of two components of comparable amplitude. Figure 4 shows the peak flux density of the Orion super water maser feature determined from our polarization observations, as a function of time from 1980 February to 1987 June. The time variations of the flux density are characterized by several outbursts, in which the flux density increases by factors of 3–5 on time scales of $\sim$2–4 months, followed by slower decays ($\sim$1 yr) to the initial levels, superposed

TABLE 2

OBSERVED PARAMETERS OF THE ORIOH SUPER H_2O MASER (1986–1987)

		Feature 1					Feature 2				
Date	Day Number	Flux Density (10^5 Jy)	Center Velocity (km s^{-1})	Line Width (km s^{-1})	P.A.	Degree Polarization (%)	Flux Density (10^5 Jy)	Center Velocity (km s^{-1})	line Width (km s^{-1})	P.A.	Degree Polarization (%)
1986 Apr 10	2292	4.96	7.81	0.44	−11°6	46.1	1.63	6.91	0.58	−24°6	50.9
1986 Apr 26	2308	5.71	7.81	0.44	−11.9	44.9	2.03	6.91	0.56	−24.6	51.2
1986 Jul 6	2379	5.50	7.75	0.45	−12.1	39.2	3.01	6.91	0.50	−24.3	51.1
1986 Aug 8	2412	4.88	7.72	0.45	−12.1	37.4	3.05	6.92	0.48	−24.8	51.0
1986 Sep 20	2455	3.38	7.68	0.45	−11.2	35.2	2.38	6.92	0.45	−25.0	51.3
1986 Oct 20	2485	2.96	7.64	0.43	−9.2	35.0	2.00	6.90	0.45	−24.8	49.8
1986 Nov 10	2506	2.71	7.62	0.42	−10.1	35.1	1.97	6.90	0.44	−26.9	49.1
1986 Dec 27	2553	2.29	7.58	0.42	−7.5	37.6	1.65	6.89	0.44	−24.1	49.8
1987 Jan 26	2583	1.83	7.56	0.39	−7.8	36.8	0.66	6.89	0.44	−23.0	49.3
1987 Feb 16	2604	1.54	7.56	0.39	−7.2	35.4	0.43	6.89	0.44	−22.2	46.9
1987 Mar 8	2624	1.79	7.55	0.40	...	...	0.41	6.89	0.43	...	...
1987 Apr 8	2655	1.08	7.54	0.41	−7.3	35.5	0.32	6.89	0.43	−21.6	47.6
1987 May 6	2683	0.79	7.54	0.44	−6.2	36.7	0.28	6.89	0.42	−22.1	47.3
1987 Jun 3	2711	0.75	7.54	0.45	−6.0	35.6	0.31	6.90	0.42	−23.1	44.9

on a "quiescent" level of $\sim 5 \times 10^5$ Jy. Such a behavior is similar to that observed in W3(OH) by Burke, Giuffrida, and Haschick (1978). For the strongest outburst, the flux density reached a value of 6.7×10^6 Jy or 0.02 $L_\odot$ in a 45 kHz wide line. On several occasions, the time between measurements was less than a week (see Table 1). We never saw large variations on this time scale. Our measurements of the long-term variations generally agree with those observed by Abraham, Vilas Boas, and del Ciampo (1986) during times of mutual observation.

b) Short-Term Flux Density Variations

Figure 5 shows the flux density of the super maser and one of the reference features as a function of time over a period of 5 hr. The data points were obtained from analog total power measurements of 90 s integration time each, made on 1980 January 15. The observed relative rms of the antenna temperature ($\Delta T_A/T_A$), with the linear trend removed, in the line channel was 6×10^{-3}, twice the theoretical rms deviation. The higher noise is probably due to short-term variations induced by jitter in the antenna tracking. The overall 5% linear trend over a period of 5 hr were probably due to a continuous drifting in the pointing position of the antenna. The ratio of the flux density of the flare feature to the flux of the nearby maser feature at 17.5 km s^{-1}, which are separated by a few arcseconds (Genzel *et al.* 1981), stayed approximately constant, with an rms of $\sim 1\%$ (see Fig. 5). We saw no evidence of variability on a time scale of a few minutes, such as that reported for 1979 November by Matveenko, Kogan, and Kostenko (1980), nor variability on a time scale of a few hours to a day, such as that reported by Abraham, Vilas Boas, and del Ciampo (1986). The

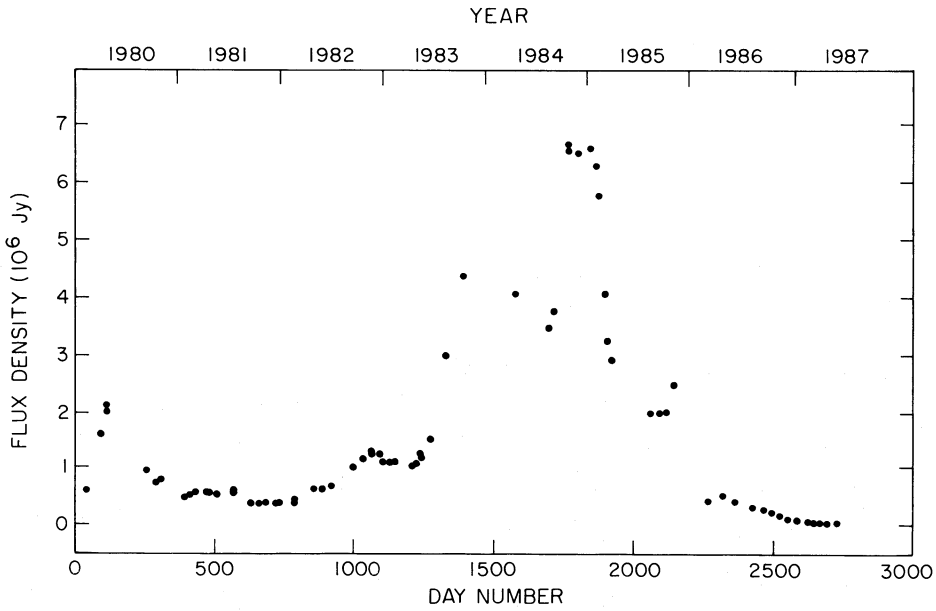

FIG. 4.—Flux density of the Orion super water maser feature plotted as a function of time, from 1980 February to 1987 June. The day numbers start at 1980 January 1.

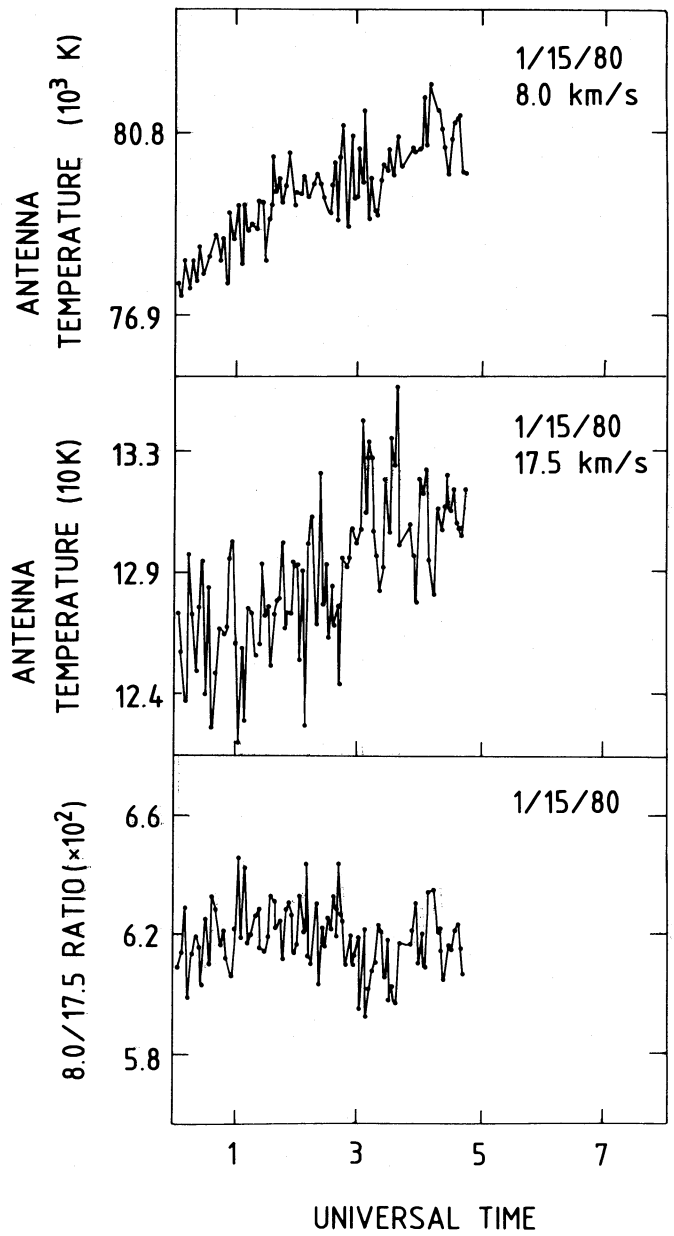

FIG. 5.—*Top and middle panels:* flux density of the super maser (at 8.0 km s^{-1}) and the 17.5 km s^{-1} feature, respectively, plotted as a function of time, between 0^h UT and 5^h UT on 1980 January 15. Integration time per data point was 90 s. *Bottom:* the flux density ratio of the super maser and 17.5 km s^{-1} features.

relaxation oscillations predicted by Montes (1977) for masers with $T_b > 10^{15}$ K, caused by the induced Compton interaction between the maser radiation and the surrounding plasma, are not observed by us, probably because of the low level of ionization.

c) Polarization

Figure 6 shows the polarization angle and degree of polarization as a function of time, from 1980 February to 1987 June. The polarization angle linearly decreased from $-18°$ in 1980 February to $-38°$ in 1981 July and since then has steadily increased, reaching a value of $-6°$ in 1987 June as the maser faded away. Furthermore, before the maser split into two components in 1986 June, the polarization angle increased as the flux density increased but reached a limiting value of $\sim -15°$ (see Fig. 7).

The degree of linear polarization as a function of the logarithm of the flux density is shown in Figure 8. For the times when the maser was strong (i.e., greater than 5×10^5 Jy), the degree of polarization decreased as the flux density increased. This result is expected if the maser stimulated emission rate exceeds the Zeeman frequency, as discussed in § IV*b*(iv). Abraham *et al.* (1981) measured the degree of polarization on 13 occasions. Three of their points were low at low flux density, which led them to suggest that the degree of linear polarization increased as the flux density increased; however, the correlation in their data is not statistically significant.

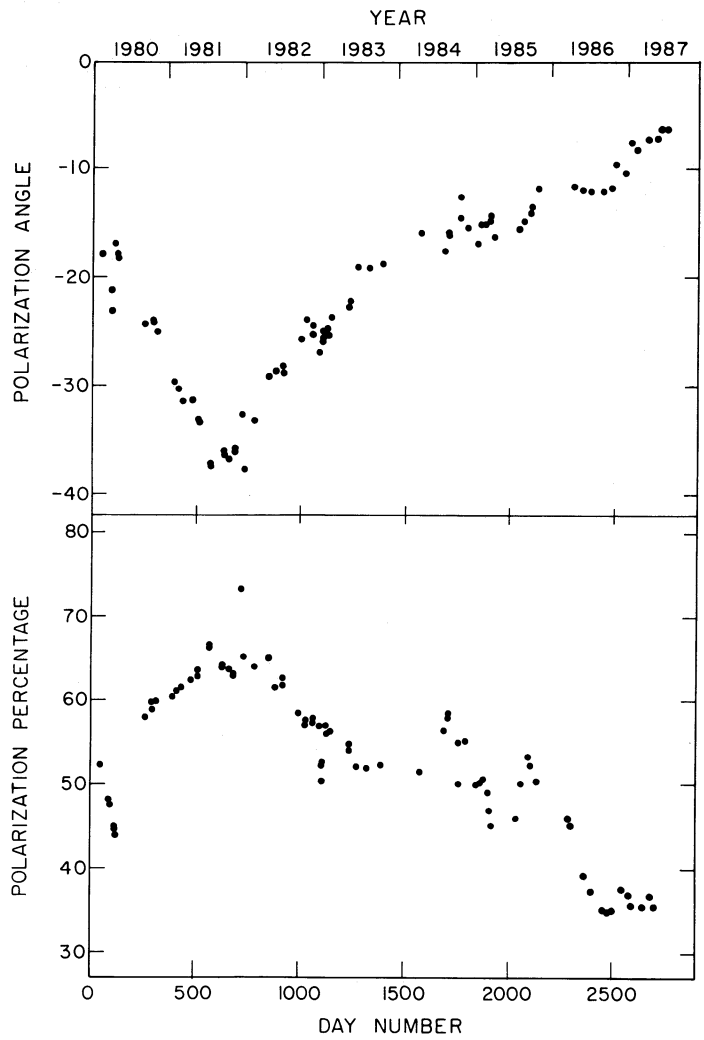

FIG. 6.—Polarization parameters of the Orion super water maser. *Top:* polarization angle plotted as a function of time. *Bottom:* degree of linear polarization plotted as a function of time. The data after 1986 January 1 refer to feature 1 (see Table 2).

d) Center Velocity, Line Width, and Line Shape

Figure 9 shows the half-power line width and center velocity of the super maser feature as a function of time from 1980 February to 1987 June. The center velocity exhibits smooth variations, changing by ~ 0.2 km s^{-1} on time scales of ~ 1 yr. The line width varies gradually with time, increasing or decreasing by as much as 30% during the observed time span. In particular, there is no significant correlation between the line width and the flux density (see Fig. 10). Note that for an unsaturated maser feature one would expect the logarithm of the flux density to be proportional to Δv^{-2} (e.g., Strelnitskii 1982, 1988).

Most likely, the line width and the center velocity variations are due to blending of two or more features. Figure 11 shows the magnitude of the difference in line center velocity between two consecutive epochs, $|v_{i+1} - v_i|$, versus the magnitude of the relative flux density variations, $|S_{i+1} - S_i|/(S_{i+1} + S_i)$, where the subscript i denotes the epoch. The values for the period (days 1400–1800) in which we had a poor temporal sampling are not plotted in Figure 11. The correlation exhibited in this figure suggests that the variations in the line center velocity are due to the variability of one or more components within a blend of maser features rather than due to physical motions of the maser cloud. Further support to this suggestion is provided by the observed line profile of the super maser. For instance, during the period from 1980 September to 1981 May, the spectral data were best fitted by two Gaussian components having a mean velocity separation of 0.3 km s^{-1} and whose relative amplitude varied with time.

We see no evidence for the presence of more than one hyperfine component of the 6_{16}–5_{23} transition. The principal hyperfine components of this transition form a triplet ($F = 7 \rightarrow 6$, $F = 6 \rightarrow 5$, and $F = 5 \rightarrow 4$) with relative frequencies of -32, 0, and $+43$ kHz (0.44, 0, and -0.58 km s^{-1}) and relative amplitudes of 0.37, 0.32, and 0.27 (e.g., Kukolich 1969; Deguchi and Watson 1986). On the basis of a statistical analysis of the angular distribution and velocities of water masers in W49, Walker (1984) argued for the presence of hyperfine components. Also, Moran *et al.* (1973) may have found one example of a line with two hyperfine components. Little additional evidence has been obtained for the presence of multiple hyperfine components. The Orion super maser is narrow enough that two or more hyperfine lines of comparable strength would be resolved in frequency. This is not observed. Note that in 1986 and 1987 (Table 2 and Fig. 3), the maser had two components with a separation approximately equal to that of the $F = 6 \rightarrow 5$

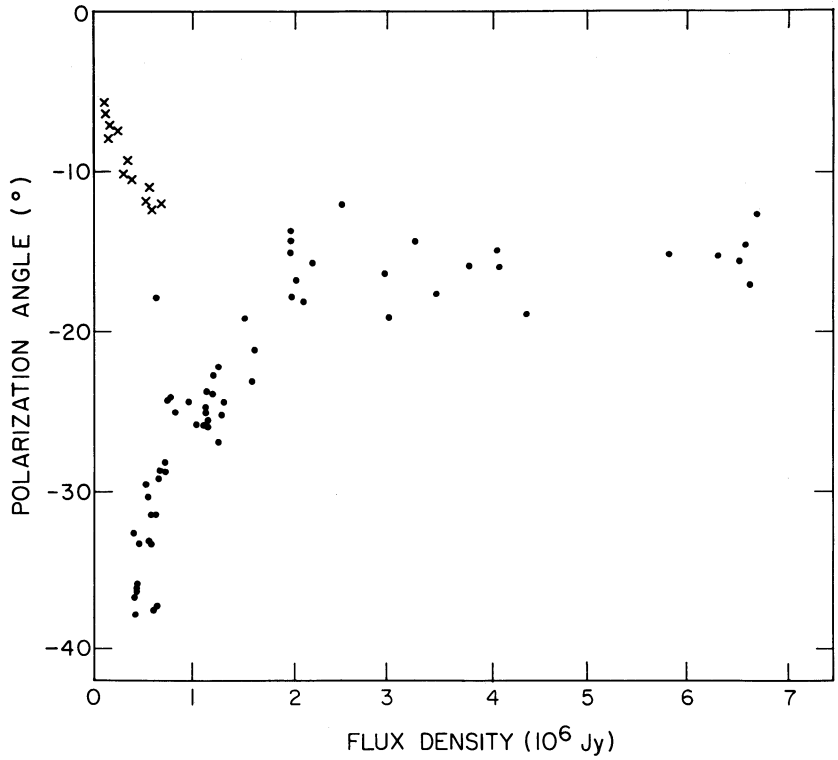

FIG. 7.—Polarization angle vs. the flux density. The dots refer to data before 1986 January 1; the crosses refer to feature 1 after 1986 January 1.

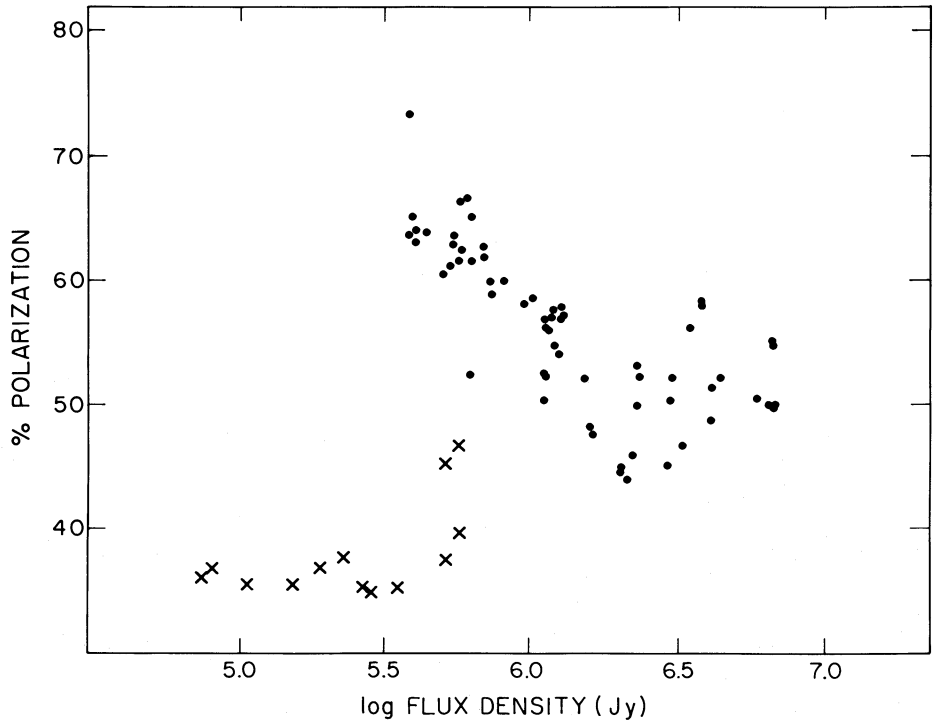

FIG. 8.—Degree of linear polarization plotted as a function of the logarithm of the flux density. The dots refer to data before 1986 January 1; the crosses refer to feature 1 after 1986 January 1.

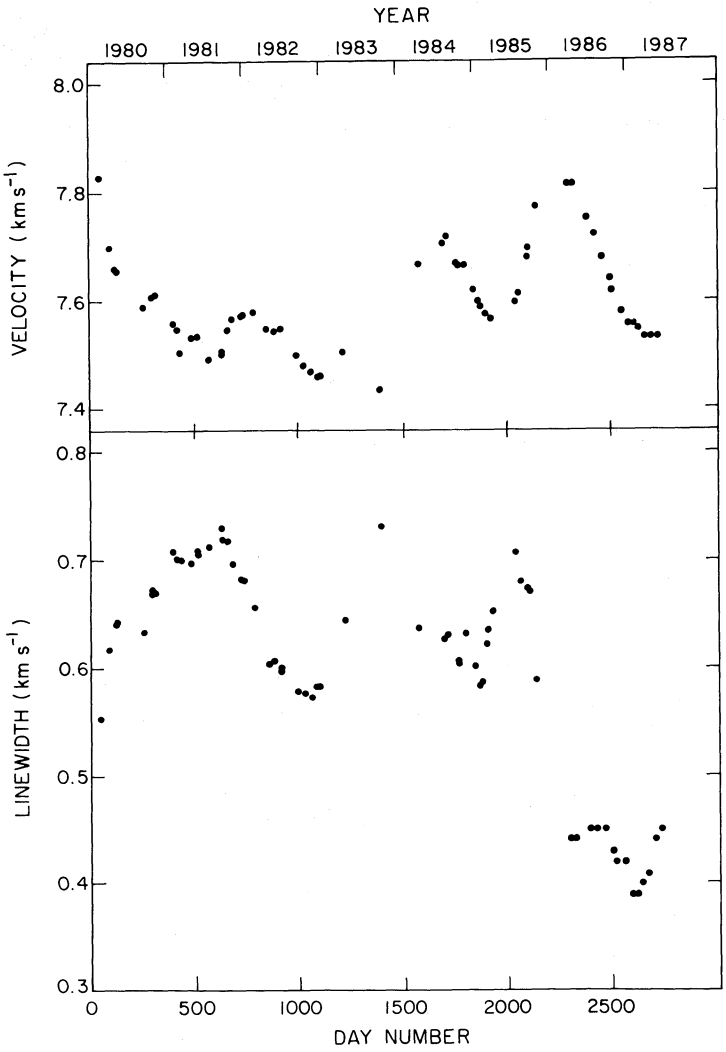

FIG. 9.—*Top:* line width (full width at half-power) of the flare feature plotted as a function of time. *Bottom:* center velocity of the flare feature plotted as a function of time. The velocity is referred to the local standard of rest and a rest frequency of 22235.08 MHz.

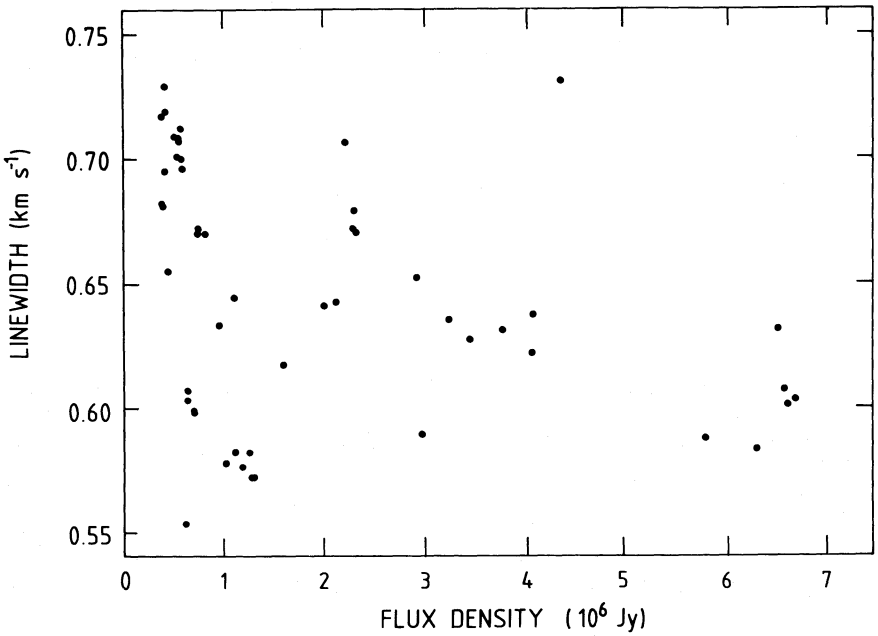

FIG. 10.—The line width vs. flux density for the Orion super maser before 1986 January 1. After 1986 January 1, the line widths were much smaller (see Table 2).

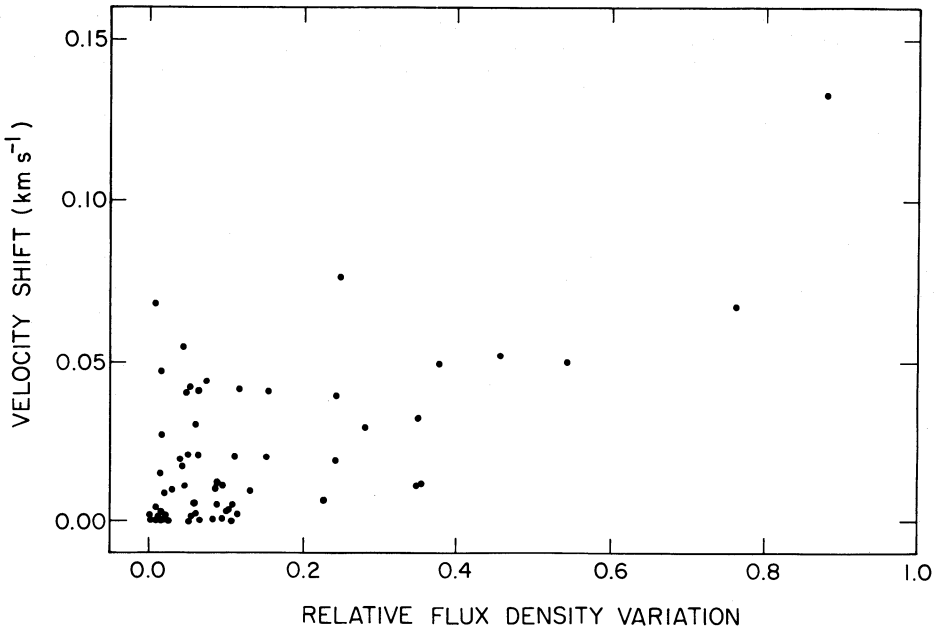

FIG. 11.—Magnitude of the change in the center velocity of the Orion super water maser feature between two consecutive epochs, ($|v_{i+1} - v_i|$), plotted vs. the magnitude of the relative variation in its flux density $|S_{i+1} - S_i|/(S_{i+1} + S_i)$.

and $F = 5 \rightarrow 4$ lines (0.58 km s^{-1}). However, the stronger component drifted in velocity by 0.3 km s^{-1} while the weaker one remained steady. Hence, these components are unlikely to be a hyperfine pair. We assume, in the absence of other evidence, that the emission is associated with the strongest hyperfine component ($F = 7 \rightarrow 6$).

e) Position

The position of the flare feature, determined in 1982 April with the VLA in its A configuration, was

$$\alpha = 05^{h}32^{m}46^{s}.64 \pm 0^{s}.01 \; ; \qquad \delta = -5°24'29''.8 \pm 0''.1 \; (1950)$$

The 1 σ errors are dominated by uncertainties in the position of phase calibrator, 0539−057. The super maser lies at an angular distance of 2".7 (~1300 AU) and 8".1 (~4000 AU) from IRc4 and IRc2, respectively.

IV. DISCUSSION

a) Observational Constraints for a Maser Model

Goldreich and Keeley (1972) have investigated models of homogeneous maser clouds having spherical and tube-shape geometries for all degrees of saturation. Such theoretical models are based on a large number of parameters, some of which cannot be measured. In the Appendix, we present a summary of the main results obtained for a model of a uniformly saturated spherical maser, and we derive a relation between model and observed parameters. In this section, we discuss the values of the model parameters that can explain the observations of the Orion water maser flare feature. Only saturated maser emission is considered since several arguments (see Reid and Moran 1981; see also discussion below) indicate that the super maser is saturated.

The basic equation for water maser radiation is given by (see eq. [A14] of the Appendix)

$$\left(\frac{n_{12}}{10^5 \text{ cm}^{-3}}\right)\left(\frac{P_e}{0.01}\right)^{7/4} = 0.99\left(\frac{S}{10^6 \text{ Jy}}\right)\left(\frac{\Delta v}{50 \text{ kHz}}\right)\left(\frac{\theta_s}{\text{mas}}\right)^{-3}\left(\frac{D}{\text{kpc}}\right)^{-1}, \tag{3a}$$

for $n_{H_2} \leq 10^{11}$ cm^{-3}, and

$$\left(\frac{n_{12}}{10^5 \text{ cm}^{-3}}\right)^{11/4}\left(\frac{P_e}{0.01}\right)^{7/4}\left(\frac{x}{10^{-6}}\right)^{-7/4} = 0.99\left(\frac{S}{10^6 \text{ Jy}}\right)\left(\frac{\Delta v}{50 \text{ kHz}}\right)\left(\frac{\theta_s}{\text{mas}}\right)^{-3}\left(\frac{D}{\text{kpc}}\right)^{-1}, \tag{3b}$$

for $n_{H_2} \leq 10^{11}$ cm^{-3}, where the model parameters are n_{H_2}, the hydrogen density; n_{12}, the total number density of the maser levels; P_e, the pump efficiency; and x, n_{12}/n_{H_2}; and where the observed parameters are S, the flux density; Δv, the line width of the maser radiation; and θ_s, the angular diameter of the maser cloud. The model assumptions are that the radiation arises in a spherically symmetric saturated cloud, and that the decay rate from the maser states, Γ, is 1 s^{-1} for molecular densities below 10^{11} cm^{-3} and $10^{-11} \times n_{H_2}$ for densities above that value.

Equations (3) allow us to derive the physical parameters of the water maser cloud in terms of two model parameters, here taken to be P_e and x. Table 3 shows derived parameters of the super maser cloud for a sequence of models with increasing pump efficiency (P_e in the range 0.001–0.1) and decreasing n_{12}/n_{H_2} ratio. The observational parameters used in the calculations were those observed in 1980 April, namely a flux density of 2×10^6 Jy, a line width of 47.5 kHz, and an apparent angular size, from VLBI observations, of 1

TABLE 3

SPHERICAL SATURATED WATER MASER MODEL[a]

Model Parameter P_e[b] (1)	Derived Parameters n_{12}[c] (10^4 cm^{-3}) (2)	n_{H_2}[d] (10^9 cm^{-3}) (3)	Γ[e] (s^{-1}) (4)	Δn_0[f] (10^2 cm^{-3}) (5)	$\lvert T_{0ex}\rvert$[g] (K) (6)	R[h] (10^{14} cm) (7)	Ω_0[i] (10^{-3} sr) (8)	W[j] (s^{-1}) (9)	B[k] (mG) (10)	Δv_A[l] (km s^{-1}) (11)
				$n_{12}/n_{H_2} = 10^{-5}$						
0.001	300	300	3.0	30.4	530	1.4	2.1	2230	12	0.04
0.003	150	150	1.5	45.3	180	1.6	1.7	1820	8	0.04
0.01	37	37	1.0	37.8	53	1.9	1.2	1220	5	0.05
0.03	5.5	5.5	1.0	16.5	18	2.6	0.7	710	4	0.10
0.1	0.7	0.7	1.0	6.7	5	3.5	0.4	390	3	0.22
				$n_{12}/n_{H_2} = 10^{-6}$						
0.001	70	700	7.0	7.0	530	1.8	1.4	1460	15	0.03
0.003	35	350	3.5	10.5	180	2.0	1.1	1200	10	0.03
0.01	16	160	1.6	16.2	53	2.2	0.9	960	6	0.03
0.03	5.5	55	1.0	16.6	18	2.6	0.7	700	4	0.03
0.1	0.7	6.5	1.0	6.7	5	3.5	0.4	390	3	0.07
				$n_{12}/n_{H_2} = 10^{-7}$						
0.001	16	1600	16.2	1.6	530	2.2	0.9	960	19	0.03
0.003	8.1	810	8.1	2.4	180	2.4	0.7	790	12	0.03
0.01	3.7	370	3.7	3.8	53	2.7	0.6	630	7	0.02
0.03	1.9	190	1.9	5.6	18	3.0	0.5	520	5	0.02
0.1	0.7	70	1.0	6.7	5	3.5	0.4	390	3	0.02

[a] The measured parameters are: flux density, 2×10^6 Jy; line width, 47.5 kHz; apparent (observed) angular size, 1.0 mas; and distance, 0.5 kpc (i.e., values observed in 1980 April). The maser luminosity is 2.8×10^{31} ergs s^{-1}.
[b] Pump efficiency.
[c] Maser level population (eq. [A14]).
[d] Hydrogen density.
[e] Decay rate from maser levels (eq. [A13]).
[f] Unsaturated population inversion (eq. [A2]).
[g] Unsaturated excitation temperature (eq. [A7]).
[h] True maser cloud radius (eq. [A6]).
[i] Beam solid angle (eq. [A5]).
[j] Microwave emission rate (eq. [5]).
[k] Magnetic field, lower limit estimate, based on the requirement of eq. (10).
[l] Alfvén broadening.

mas (Matveenko, Moran, and Genzel 1982). The total density of water maser levels, n_{12}, is derived from equation (3). Other model parameters such as the unsaturated population inversion, Δn_0, unsaturated excitation temperature, T_{0ex}, radius of maser cloud, R, and beam solid angle of the maser radiation, Ω_0, are given in columns (5)–(8) of Table 3, respectively (see the Appendix). The maser luminosity $\mathscr{L}$ emitted by the spherical cloud is independent of model parameters and equal to 2.9×10^{31} ergs s^{-1}.

b) Derived Parameters

i) *Saturation State*

A usual question that arises in the discussion of interstellar masers is, Are the masers saturated or unsaturated? The brightness temperature at which water masers saturate is (see Reid and Moran 1981)

$$T_s^{H_2O} = 3.5 \times 10^9 \left(\frac{\Gamma + 2C}{\Omega_0^*} \right), \tag{4}$$

where C is the collision rate across the maser levels, and Ω_0^* is the beam solid angle of the maser emission at the surface of a just saturated maser cloud. The most uncertain parameter in the determination of the saturation temperature is the beam solid angle Ω_0^*; however, it is unlikely that $\Omega_0^* < 10^{-2}$ sr. For an unsaturated sphere, $\Omega_0^* \sim (2\alpha R)^{-1}$, where $2\alpha R$ is the gain (Reid and Moran 1981). Since $2\alpha R$ is unlikely to be greater than 50, then $\Omega_0^* > 2 \times 10^{-2}$ sr. To be conservative, we adopt a lower value for the beam solid angle at the surface of an unsaturated maser of 10^{-2} sr and an upper limit value for the collisional rates of 10 s^{-1} and find $T_s^{H_2O} \sim 3.5 \times 10^{12}$ K. For the epoch of 1979 November, the angular diameter was 1 mas and the flux density was 1.7×10^6 Jy (Matveenko, Moran, and Genzel 1982), which gives a brightness temperature of 4×10^{15} K. Therefore, the maser emission from the super feature is probably saturated.

ii) *Kinetic Temperature*

The simple theory of maser line widths predicts line narrowing during unsaturated amplification and rebroadening, to the full Dopper width, during saturated amplification. Thus, if the maser is saturated, the observed line width allows us to compute the kinetic temperature of the gas.

Goldreich and Kwan (1974*b*) showed, however, that rebroadening of the line during saturated growth can be inhibited due to infrared line radiation trapped between the maser levels and other rotational levels. Line rebroadening does not occur provided that the cross relaxation rate, γ, exceeds the stimulated emission rate per molecule across the maser level, W. For H_2O masers, W can be written, in terms of observable quantities, as

$$W = 530\left(\frac{S}{10^6\ \mathrm{Jy}}\right)\left(\frac{\theta_s}{\mathrm{mas}}\right)^{-2}\left(\frac{\Omega_0}{10^{-3}}\right)\mathrm{s}^{-1}\ , \tag{5}$$

where Ω_0 is the solid angle into which the maser radiation is beamed. In particular, for the Orion super feature, using the flux density observed on 1980 April 23 ($S = 2 \times 10^6$ Jy), and adopting $\theta_s = 1.0$ mas, we find $W \sim 1 \times 10^3(\Omega_0/10^{-3})\ \mathrm{s}^{-1}$. The values of the beam solid angle of the maser radiation, derived from completely saturated spherical maser (hereafter CSSM) models fitting the 1980 April observations, are greater than 10^{-4} sr (see col. [8] of Table 3); therefore, we conclude that $W > 100\ \mathrm{s}^{-1}$. For the H_2O molecule, the maser levels are coupled to other rotational levels by far-infrared resonances; thus, the cross relaxation rate γ is $\sim kTA_c/30h\nu_{\mathrm{FIR}}$ (Goldreich *et al.* 1973*b*). A typical value for the Einstein coefficient A_c is $1\ \mathrm{s}^{-1}$; thus, $\gamma \sim 2\ \mathrm{s}^{-1}$, and $\gamma \ll W$, at temperatures of several hundred degrees. Therefore, the trapping of infrared radiation will not have any effect on the line profile and the line width should be the full Dopper width.

On the assumption that the observed line width can be used to determine the kinetic temperature T_K of the Orion super feature maser cloud, the average value of the line width, of 0.6 km s^{-1} (45 kHz), implies $T_K \sim 150$ K. Note that the maser transition lies 640 K above the ground state so that the maser levels cannot be significantly populated by normal thermal collision processes. The line width variations associated with the super feature (Fig. 9) could be explained by variations of the kinetic temperature of the gas in the range $120 < T_K < 210$. We feel, however, that the most likely interpretation for these variations is blending of a few maser features that vary in strength.

Under certain conditions, the line width of maser features might be broadened by the presence of strong magnetic fields, through either the Zeeman effect or by Alfvén turbulence, and by strong electric fields through the Stark effect. For the Orion super water feature ($T_B \sim 5 \times 10^{15}$ K, $\Omega_0 \sim 10^{-3}$ sr), the expected broadening due to the resonant Stark effect (see Genzel *et al.* 1979) is ~ 2 kHz, considerably smaller than the line width of the maser radiation. On the other hand, the strength of the magnetic field of the maser cloud, derived from the polarization observations (see § IV*b*[iv]), is < 1 G, implying a Zeeman splitting of less than 1 kHz. Thus, Stark and Zeeman broadening are negligible for the super water feature. Broadening of the line due to Alfvén turbulence (Myers and Goodman 1988) might conceivably be important at the magnetic field strengths and densities associated with the super maser cloud. The values of the broadening (FWHM) due to Alfvén turbulence, $\Delta v_{\mathrm{A}} = (8 \ln 2/12\pi\mu)^{1/2} B n_{\mathrm{H}_2}^{-1/2}$, where μ is the mean molecular mass, are given in column (11) of Table 3. They are generally smaller than 0.05 km s^{-1}, and thus Alfvén broadening is probably negligible.

iii) *Luminosity*

The number of photons per second, N_m, emitted by a water maser cloud can be expressed in terms of the observed flux density and line width as (see Moran 1982)

$$N_m = 4 \times 10^{47}\left(\frac{S}{10^6\ \mathrm{Jy}}\right)\left(\frac{\Delta v_m}{50\ \mathrm{kHz}}\right)\left(\frac{\Omega_m}{4\pi}\right)\left(\frac{D}{1\ \mathrm{kpc}}\right)^2\ \mathrm{s}^{-1}\ , \tag{6}$$

where Ω_m is the solid angle into which the maser cloud radiates, in general different from the solid angle, Ω_0, into which the maser radiation from a given surface element is beamed. For the Orion water maser flare, on the assumption that it emits isotropically (i.e., $\Omega_m = 4\pi$), we find that $N_m = 6 \times 10^{47}\ \mathrm{s}^{-1}$ at the epoch of maximum flux density. The luminosity is $2.2 \times 10^{-2}\ L_\odot$.

The large number of maser photons emitted by the super water maser places a significant constraint on the pump energy source and pump mechanisms. Radiative pumping mechanisms require at least one pumping photon per maser photon (see Forster, Welch, and Wright 1977). The pump photons may be supplied either by an external or an internal source. If the pumping is accomplished by radiative excitation, then the observed maser flux density implies that the pump source should have a flux density, S_p, at the pump line frequency, ν_p, of

$$S_p \geq 10^7\left(\frac{\Omega_m}{\Omega_p}\right)\left(\frac{\Delta v_m}{v_m}\right)\left(\frac{\nu_p}{\Delta v_p}\right)\mathrm{Jy}\ , \tag{7}$$

where Ω_p is the solid angle subtended by the maser seen from the pump source and Δv_p is the line width of the pump line. The ratio of the maser to pump fractional bandwidth ratio depends on the details of the pump mechanism; however, for a saturated maser, it is likely to be close to unity. Although most of the H_2O maser features in the Orion-KL region arise from condensations in the outflow emanating from IRc2 (Genzel *et al.* 1981), neither IRc2 nor the nearby IRc4 are likely to radiatively pump the flare feature. The flux densities at 20 μm of IRc2 and IRc4 are ~ 300 and 600 Jy, respectively (Downes *et al.* 1981). Since IRc2 and IRc4 are rather distant from the maser cloud, $\Omega_p < 10^{-3}$, we conclude that neither of these objects are likely to be the pump source. If the pump photons are supplied by an internal energy source (i.e., $\Omega_p = 4\pi$), then for a spherical maser (i.e., $\Omega_m = 4\pi$) we find $S_p \sim 10^7$ Jy. This value greatly exceeds the upper limits on the flux density in the vicinity of the super maser, of $\sim 10^3$ Jy at ~ 20 μm (Downes *et al.* 1981; Wynn-Williams *et al.* 1984).

In order to reduce the estimate of the required luminosity of the pump source, we could relax the assumption of spherical symmetry and assume that the masers do not emit isotropically. For example, in a cylindrical geometry, $\Omega_m \ll 4\pi$ because strong emission occurs along rays that traverse the entire length of the cylinder so that $\Omega_m \sim \pi(l/L)^2$, where l is the radius and L the length of the cylinder; L is unlikely to be greater than 40 times l. Therefore, $\Omega_m \gtrsim 10^{-3}$ and $S_p \gtrsim 10^3$ Jy.

The most likely source of excitation is collisional. Goldreich and Kwan (1974*a*) have shown that for collisional pumps in which the heat sink is achieved by radiative decay, the radius of the maser cloud is related to the photon maser output by

$$\left(\frac{R}{10^{16}\ \mathrm{cm}}\right) = 0.65\left(\frac{N_m}{10^{48}\ \mathrm{s}^{-1}}\right)^{1/2}\left(\frac{\nu_p/\Delta\nu_p}{10^5}\right)^{1/2}\left(\frac{\nu_p}{3\times 10^{13}\ \mathrm{Hz}}\right)^{-3/2}(e^{h\nu_p/kT_p}-1)^{1/2}\ , \tag{8}$$

where T_p is the excitation temperature of the pump line. Thus, to account for a maser photon rate of $\sim 10^{48}$ s^{-1}, for example, with an infrared line at 10 μm with an excitation temperature of ~ 500 K and $\nu_p/\Delta\nu_p \sim 10^5$, the cloud radius should be $\sim 10^{16}$ cm. This value is ~ 30 times larger than the model values of the radius of the flare features, derived with the CSSM model, of $\sim 3 \times 10^{14}$ cm (see col. [7] of Table 3). Thus, collisional pumps in which the heat sink is due to radiative processes usually lead to cloud sizes far greater than those derived from the observations. However, if the maser emission is not spherical and the emission is anisotropic, then the required size of the maser could be smaller. In this case, collisional pumping with a heat sink may be viable.

A possible mechanism to explain strong masers is one that involves a collisional pump and a collisional sink of the H_2O molecules due to their interaction with two kinds of particles that have different temperatures (Strelnitskii 1980, 1984; Kylafis and Norman 1986). Such a pump model is not restricted to densities below the critical density of 10^{11} cm^{-3} required by collisional pump models that rely on gas and dust at different temperatures.

iv) *Magnetic Fields*

The polarization characteristics of maser radiation depend on the relative sizes of the stimulated emission rate W, the decay rate of the maser levels Γ, the Zeeman splitting Z, the maser bandwidth, $\Delta\nu$, and the cross relaxation rate γ. The water molecule is a nonparamagnetic asymmetric top molecule and thus interacts only weakly with an applied external field. The characteristic Zeeman splitting between σ components is given by $2\mu_0 g_1 B/h$, where $\mu_0 = (eh/4\pi m_p c)$ is the nuclear magneton, g_1 is the Landé factor of the lower level, and B is the external magnetic field. For the water molecule, $g_1 = 0.696$ (Kukolich 1969); thus

$$Z \approx 1 \times 10^3\left(\frac{B}{\mathrm{G}}\right)\ \mathrm{Hz}\ . \tag{9}$$

Magnetic fields of ~ 50 G, much larger than those expected at the densities of water maser clouds, are required for the Zeeman splitting to equal the Doppler width of the lines. Thus, the typical bandwidth of the water maser radiation is likely to be much greater than the Zeeman splitting. In this case, GKK predicted that the emitted radiation should be linearly polarized if (1) $W > \Gamma$, (2) $W > \gamma$, and (3) $(W\Gamma)^{1/2} < 2\pi Z$, and unpolarized otherwise. The first condition means that the maser is saturated and the second condition that infrared trapping is negligible.

For the water molecule, $\Gamma \sim 1$–10 s^{-1}, $\gamma \sim 2$ s^{-1}, and $Z \sim 10^3 B$ Hz (B in Gauss). In particular, for the Orion super water maser feature, $W \sim 2 \times 10^3(\Omega_0/10^{-3})$ s^{-1} (see eq. [5]); thus, $W > \Gamma$, and $W > \gamma$ for all reasonable values of Ω_0 (see Table 3, cols. [8] and [9]). Therefore, the first two conditions for linear polarization are satisfied by the Orion super maser. Since the maser emission is highly polarized, it implies that $2\pi Z > (W\Gamma)^{1/2}$, which can be written, in terms of observable quantities, by use of equation (5) as

$$B > 3.5\left(\frac{S}{10^6\ \mathrm{Jy}}\right)^{1/2}\left(\frac{\theta_s}{\mathrm{mas}}\right)^{-1}\left(\frac{\Omega_0}{10^{-3}\ \mathrm{sr}}\right)^{1/2}\left(\frac{\Gamma}{\mathrm{s}^{-1}}\right)^{1/2}\ \mathrm{mG}\ . \tag{10}$$

Column (10) of Table 3 gives lower limits of the magnetic field strength in the Orion maser cloud derived from the above polarization requirement, using the values of S observed in 1980 April, $\theta_s = 1$ mas, and the values of Ω_0 and Γ derived within the CSSM model. This calculation suggests that the magnetic field strength associated with the Orion super maser cloud is greater than 10 mG, to ensure linearly polarized emission.

An additional estimate of B can be set because the degree of polarization is large. For saturated masers, degrees of linear polarization greater than $\frac{1}{3}$ can be achieved only if $2\pi Z > W$ (GKK; Deguchi and Watson 1986). Thus, for a saturated maser cloud embedded in a magnetic field B, there is a maximum stimulated emission rate, W_m, given by

$$W_m = 4\pi\mu_0 g_1 B/h\ , \tag{11}$$

above which the degree of polarization will decrease. For the water molecule, $W_m = 6.7B$, where W_m is in s^{-1} and B is in milliGauss.

The degree of polarization of the super maser feature was $\sim 60\%$, suggesting that $2\pi Z > W$. Further, at large flux densities, the degree of polarization of the super feature decreased as the flux density increased (see Fig. 8). This trend can most easily be explained if $W > W_m$ at the largest flux densities. We suggest that, in the range of flux densities encompassed by our observations, the stimulated emission rate of the super water maser is comparable to the Zeeman splitting frequency. In particular, as can be seen in Figure 8, the degree of polarization decreases for flux densities above 4×10^5 Jy, which corresponds to $W_m \simeq 200$ s^{-1} for $\Omega_0 = 10^{-3}$ and $\theta_s = 1$ mas. Hence, the estimate of the magnetic field based on this criterion is 30 mG. We adopt this value as the magnetic field for the super maser. The Alfvénic line broadening for this field and $n_{H_2} = 5 \times 10^{11}$ cm^{-3} is a negligible 0.08 km s^{-1}. The attempt to make a direct measurement of the Zeeman splitting in the Orion super maser by Fiebig and Güsten (1988) gave the result $B < 71$ mG. We emphasize that our value for the magnetic field depends on our assumption that the linear polarization is caused by magnetic fields (i.e., anisotropic radiative pumping can cause linear polarization with no static magnetic field; Western and Watson 1983), and on our assumption about the maser geometry from which we deduced the value of the beam angle.

A magnetic field strength of at least 30 mG at the molecular densities of the water maser cloud is plausible on the basis of observed magnetic fields at lower densities and theoretical expectations. Scaling the typical magnetic field strength of ~ 5 mG derived from the Zeeman pattern in OH maser clouds at densities of $\sim 10^7$ cm^{-3} (Moran *et al.* 1978), to the molecular density of the

water vapor maser clouds of $\sim 10^{11}$ cm^{-3} gives $B \sim 0.5$ G if we assume $B \propto n_{H_2}^{1/2}$ (Mouschovias 1976). The polarization in the masers is undoubtedly due to the presence of magnetic fields.

GKK showed that the limiting Stokes parameters for a saturated maser, operating between $J = 1$ and $J = 0$ levels, in the case that $2\pi Z > W$ and in the absence of Faraday rotation, are given by (GKK, case 2a)

$$\begin{aligned} &Q = -I\,, \quad U = 0\,, \quad V = 0 \qquad \text{for } \sin^2\theta \le \tfrac{1}{3}\,, \\ &Q = \left(\frac{3\sin^2\theta - 2}{3\sin^2\theta}\right) I\,, \quad U = KI\,, \quad V = 0 \qquad \text{for } \sin^2\theta \ge \tfrac{1}{3}\,, \end{aligned} \tag{12}$$

where θ is the angle between the direction of the magnetic field and the line of sight, and K is a constant. In addition, Western and Watson (1984) have argued that the linear polarization should be either perpendicular or parallel to the projected direction of the magnetic field, as seen by the observer, and therefore concluded that $K = 0$ (this can also be shown in the limiting case by solving the transfer equations derived by GKK).

Detailed calculations for a unidirectional H_2O maser in the 6_{16}–5_{23} transition have been made by Deguchi and Watson (1986). They found that the maximum allowable degree of linear polarization is $\sim 70\%$, instead of the 100% allowed by GKK for the $J = 1 \rightarrow 0$ masers. Since the observed polarization approaches this limit, we can conclude that the angle between the magnetic field direction and the line of sight is $\sim 30°$ (see Fig. 2 of Deguchi and Watson 1986). In addition, the limiting polarization angle at maximum observed flux density of about $-15°$ may indicate that the projection angle of the magnetic field on the plane of the sky is $-15°$.

v) *The Outbursts*

For a saturated spherical maser cloud of radius R, the flux density can be written as (substituting eqs. [A8] and [A10] into eq. [A11])

$$S = 1.65\,\frac{h\nu}{\Delta\nu}\,P_e \Gamma n_{12}\,\frac{V}{4\pi D^2}\,, \tag{13}$$

where $V = 4\pi R^3/3$ is the maser cloud volume. This relation can be intuitively understood if we note that the steady state solution of the population equation implies that $(P_2 + P_1)(n - n_{12}) = \Gamma n_{12}$, where n is the total number density of the maser molecule species, and P_1 and P_2 are the pump rates per molecule into the maser states (Goldreich and Keeley 1972). Therefore, $P_e \Gamma n_{12} = (P_2 - P_1)(n - n_{12})$, namely, $P_e \Gamma n_{12}$ is equal to the net pump rate of the maser levels per unit volume. Hence, equation (13) tells us that each pump inversion leads to a maser photon that escapes the cloud.

Equation (13) shows that variations in the flux density can be due to changes of either the physical size of the excited region, pump rate of the maser levels, or density of the water molecules. The flux density variations associated with the Orion super feature could be most simply explained if the size of the excited region varied by factors of ~ 2. This might occur, for example, in shock-excited masers in which the energy for the maser pump propagates through a gas cloud that is irregular in shape and density. This conjecture could be tested directly with VLBI experiments.

vi) *An Interpretation of the Orion Super Water Maser*

The physical situation of the super maser is not clear. One possibility is that it is a dense fragment that is part of the general outflow from IRc2. In this case, since its Doppler velocity is near the ambient cloud velocity, the maser would have to be moving nearly transverse to the line of sight. The pump power could be derived from a collision of the fragment with a less dense clump in the ambient cloud medium. There is sufficient kinetic energy to supply the apparent isotropic luminosity of 6×10^{39} ergs, especially if the maser emission is beamed (see, e.g., Tarter and Welch 1986). The pumping could be achieved by the two stream model of Kylafis and Norman (1986, 1987) in which the electrons are at a much higher temperature than the neutral particles. Such conditions might occur in magnetohydrodynamic shocks propagating into magnetized molecular gas (Draine, Roberge, and Dalgarno 1983). The Kylafis and Norman model appears to require magnetic fields that are considerably stronger than those derived by us (30 G), which may present a problem. Their detailed numerical calculations for a model with $T_K \sim 50$ K and $T_e \sim 2000$ K give pump efficiencies of $\sim 0.2\%$. Thus, in order to explain the photon emission rate from the Orion super maser feature of $\sim 10^{48}$ s^{-1}, a total gas density, which is predominantly composed of molecular hydrogen, of $\sim 2 \times 10^{11}$ cm^{-3}, is required (see Table 3). This density is $\sim 10^4$ times larger than that found in the densest, although large scale, regions of the Orion molecular cloud (see, e.g., White *et al.* 1986), but the gas could be compressed to such large densities in the collision process.

Alternatively, the precursor maser cloud might already be a dense and small magnetized gas fragment (a protoplanetary globule) embedded in the molecular cloud possibly associated with another energy source than IRC2 (e.g., Matveenko, Graham, and Diamond 1988). Detailed calculations of MHD shocks propagating into dense (10^6 cm^{-3}), magnetized ($B \sim 1$ mG) molecular gas show that $T_e > T_H$ occurs naturally in the pre- and postshock transition region (Draine, Roberge, and Dalgarno 1983). In addition, the abundance of water is substantially increased in the postshock region. The water maser levels might then be efficiently collisionally pumped in this region by the electrons (see Kylafis and Norman 1987), giving rise to strong maser emission. Although no computations have yet been performed for the suggested preshock conditions of the Orion maser cloud, it is tempting to attribute the maser excitation to magnetohydrodynamic shock waves, possibly driven by a nearby stellar wind source, propagating through the dense magnetized clump.

We note that a flare was reported in the 183 GHz water line from the Orion-KL region, which began sometime between 1977 and 1980 (Kuiper *et al.* 1984). There may be a connection between this flare and the one at 22 GHz. Kuiper *et al.* (1984) discuss the possibilities.

V. SUMMARY

We monitored for 7 yr the most powerful water maser feature in Orion. The main results and conclusions presented in this paper are as follows.

1. The super water maser in the Orion molecular cloud was the strongest water maser ever detected, reaching a peak flux density of $\sim 6.7 \times 10^6$ Jy. If the maser radiation is isotropic, the peak luminosity emitted by the cloud in the water maser line is $\sim 3 \times 10^{31}$ ergs s^{-1}. The total radiated energy between 1979 August (the time of the first known flare of the super maser) and 1987 June was 6×10^{39} ergs.

2. Three flares occurred during the period 1980 February to 1987 June superposed on a "quiescent" flux density level of $\sim 5 \times 10^5$ Jy. In the outbursts, the flux density rapidly increased, on a time scale of ~ 2–3 months, followed by a slow decay to the quiescent level on the time scale of 1 yr. Since 1986 January, the maser has steadily declined in flux density.

3. The maser radiation was highly linearly polarized, with the degree of polarization ranging from 45% to 65%. The polarization angle shows gradual variations in time, decreasing from roughly $-20°$ in 1980 February to roughly $-37°$ in 1981 July and then increasing steadily to about $-6°$ in 1987 June. If the polarization is due to the presence of magnetic fields, the observation that the polarization is quenched at high flux densities implies a magnetic field strength of ~ 30 mG. This field strength depends on the source geometry through the maser beam angle, which we assume is 10^{-3} sr. The high degree of polarization can only be achieved if the angle between the magnetic field direction and the line of sight is $\sim 30°$. The position angle of the magnetic field direction is about $-15°$.

4. The line width and center velocity of the super maser feature varied gradually with time, changing by $\sim 20\%$ and 0.2 km s^{-1}, respectively, on time scales of ~ 1 year. These variations were most likely due to blending of two or more features that vary in strength. The kinetic temperature of the gas, derived from the maser line width on the assumption that line broadening is due to Doppler effects is ~ 150 K.

5. On the assumption that the emission arose from a saturated spherical maser cloud, the observed parameters of the maser radiation (flux density, angular size, and line width) imply molecular hydrogen densities of $\sim 10^9$–10^{11} cm^{-3} for pump efficiencies in the range of 0.1—10%. The beam solid angle of the maser radiation was $\sim 10^{-3}$ sr, and the radius of the maser cloud was $\sim 3 \times 10^{14}$ cm.

We plan to continue to monitor the super maser at Haystack Observatory although its flux density seems to be in decline ($\sim 40 \times 10^3$ Jy in 1988 May). More VLBI measurements to establish the temporal behavior of the angular size would be desirable.

We thank W. Hoffmann for building the rotating mechanism for the feed on the Haystack antenna, W. Watson and N. Kylafis for useful discussions of magnetic fields in water vapor masers, and L. J. Greenhill for carefully reading the manuscript. Radio astronomy at the Haystack Observatory is supported by the National Science Foundation under grant AST 85-12598.

APPENDIX

SPHERICAL COSMIC MASER MODEL

For a completely saturated spherical maser cloud of radius R, Goldreich and Keeley (1972) have shown that

1. There is a saturated core of radius, R_{sat}, given by

$$R_{sat} = 1.35\alpha^{1/4}R\,, \tag{A1}$$

where $\alpha = (1/P_e)(A/\Gamma)$, and $P_e = (P_2 - P_1)/(P_2 + P_1)$ is the pump efficiency, P_1 and P_2 are the pump rates per molecule into the maser states, Γ is the decay rate of the maser states, A is the Einstein spontaneous emission coefficient. The quantity P_e is given by

$$P_e = \frac{\Delta n_0}{n_{12}}\,, \tag{A2}$$

where Δn_0 is the unsaturated population inversion and n_{12} is the total population density of the two maser levels.

2. The apparent radius of the maser cloud, R_{app}, is

$$R_{app} = 0.68R_{sat}\,. \tag{A3}$$

3. The solid angle, Ω_0, into which the maser radiation is beamed, is

$$\Omega_0 = \pi\left(\frac{R_{app}}{R}\right)^2\,, \tag{A4}$$

which, using equations (A1) and (A3), can be expressed as

$$\Omega_0 = 2.65\alpha^{1/2}\,. \tag{A5}$$

4. The brightness temperature of the maser radiation is

$$T_B = 5.2\,\frac{R}{\alpha^{3/2}}\,T_{0ex}\,\frac{\lambda^2 A\,\Delta n_0}{8\pi\,\Delta v}\,, \tag{A6}$$

where T_{0ex} is the unsaturated excitation temperature, and Δv is the line width of the maser radiation. In terms of the apparent radius and using the relation between Δn_0 and T_{0ex},

$$\Delta n_0 \, T_{0ex} = (hv/2k) n_{12} \, , \tag{A7}$$

equation (A6) becomes

$$T_B = 0.113 \, \frac{hc^2}{kv} \, A \, \frac{n_{12} \, R_{app}}{\Delta v \alpha^{7/4}} \, . \tag{A8}$$

5. The energy per second, $\mathscr{L}$, emitted by the cloud at the maser frequency is

$$\mathscr{L} = 8\pi k v^2 R^2 T_B \Omega_0 \, \Delta v / c^2 \, . \tag{A9}$$

The observed quantities of the maser radiation are the line width, Δv; the observed angular diameter of the maser cloud, θ_s, which is related to the apparent radius by

$$\theta_s = \frac{2R_{app}}{D} \, , \tag{A10}$$

where D is the distance to the source; and the flux density, S, which is related to the brightness temperature by the equation

$$S = \frac{2k}{\lambda^2} \, T_B \, \frac{\pi}{4} \, \theta_s^2 \, . \tag{A11}$$

The five independent model parameters contained in the equations of the completely saturated maser cloud model are R, P_e, Γ, Δv, and n_{12}. Since there are three observed quantities, we may combine these in terms of model parameters, in one equation having three unknowns. Substituting equations (A8) and (A10) and α in terms of the pump efficiency into expression (A11), we obtain the basic equation of the saturated spherical maser model, constraining the parameters P_e, n_{12}, and Γ such that

$$n_{12}(\Gamma P_e)^{7/4} = \frac{11 A^{3/4}}{hv} \, S \theta_s^{-3} \, \Delta v D^{-1} \, , \tag{A12}$$

For the water molecule, the decay rate Γ is dominated by the spontaneous decay rate from the maser levels, of $\sim 1 \text{ s}^{-1}$, if the total molecular density is smaller than 10^{11} cm^{-3}. At larger densities, Γ is dominated by collisions with H_2 molecules; thus, $\Gamma \sim n_{H_2} \sigma v_{th}$, where n_{H_2} is the molecular hydrogen number density, v_{th} is the rms thermal velocity of the H_2 molecules, and σ is the collision cross section. On the assumption that $\sigma v_{th} \sim 10^{-11} \text{ cm}^3 \text{ s}^{-1}$ (Green 1980), we may write

$$\Gamma = \begin{cases} 1 \text{ s}^{-1} \, , & n_{H_2} \leq 10^{11} \text{ cm}^{-3} \, , \\ 10^{-11} \times n_{H_2} \text{ s}^{-1} \, , & n_{H_2} \geq 10^{11} \text{ cm}^{-3} \, . \end{cases} \tag{A13}$$

Replacing equation (A13) in (A12), the basic relation for water maser transition ($A = 1.91 \times 10^{-9} \text{ s}^{-1}$, $v = 22.235$ GHz) can be written as

$$\left(\frac{n_{12}}{10^5 \text{ cm}^{-3}}\right)\left(\frac{P_e}{0.01}\right)^{7/4} = 0.99\left(\frac{S}{10^6 \text{ Jy}}\right)\left(\frac{\Delta v}{50 \text{ kHz}}\right)\left(\frac{\theta_s}{\text{mas}}\right)^{-3}\left(\frac{D}{\text{kpc}}\right)^{-1} \, , \tag{A14a}$$

for $n_{H_2} \leq 10^{11} \text{ cm}^{-3}$, and

$$\left(\frac{n_{12}}{10^5 \text{ cm}^{-3}}\right)^{11/4}\left(\frac{P_e}{0.01}\right)^{7/4}\left(\frac{x}{10^{-6}}\right)^{-7/4} = 0.99\left(\frac{S}{10^6 \text{ Jy}}\right)\left(\frac{\Delta v}{50 \text{ kHz}}\right)\left(\frac{\theta_s}{\text{mas}}\right)^{-3}\left(\frac{D}{\text{kpc}}\right)^{-1} \, , \tag{A14b}$$

for $n_{H_2} \geq 10^{11} \text{ cm}^{-3}$, where x is the ratio of the number density of water molecules in the maser levels, n_{12}, to the number density of molecular hydrogen, n_{H_2}. Strelnitskii (1984) gives relations similar to equations (A14).

REFERENCES

Abraham, Z., Cohen, N. L., Opher, R., Rafaelli, J. C., and Zisk, S. H. 1981, *Astr. Ap. Letters*, **100**, L10.
Abraham, Z., Opher, R., and Rafaelli, J. C. 1979, *IAU Circ.*, No. 3415.
Abraham, Z., Vilas Boas, J. W. S., and del Ciampo, L. F. 1986, *Astr. Ap.*, **167**, 311.
Burke, B. F., Giuffrida, T. S., and Haschick, A. D. 1978, *Ap. J. (Letters)*, **226**, L21.
Deguchi, S., and Watson, W. D. 1986, *Ap. J.*, **302**, 750.
Downes, D., Genzel, R., Becklin, E. E., and Wynn-Williams, C. G. 1981, *Ap. J.*, **244**, 869.
Draine, B. T., Roberge, W. G., and Dalgarno, A. 1983, *Ap. J.*, **264**, 485.
Fiebig, D., and Güsten, R. 1989, *Astr. Ap.*, in press.
Forster, J. R., Welch, W. J., and Wright, M. C. H. 1977, *Ap. J. (Letters)*, **215**, L121.
Garay, G. 1983, Ph.D. thesis, Harvard University.
Garay, G., Moran, J. M., and Reid, M. J. 1987, *Ap. J.*, **314**, 535.
Genzel, R., and Downes, D. 1977, *Astr. Ap. Suppl.*, **30**, 145.
Genzel, R. *et al.* 1979, *Astr. Ap.*, **78**, 239.
Genzel, R., Reid, M. J., Moran, J. M., and Downes, D. 1981, *Ap. J.*, **244**, 884.
Goldreich, P., and Keeley, D. A. 1972, *Ap. J.*, **174**, 517.
Goldreich, P., Keeley, D. A., and Kwan, J. 1973*a*, *Ap. J.*, **179**, 111 (GKK).
———. 1973*b*, *Ap. J.*, **182**, 55 (GKK).
Goldreich, P., and Kwan, J. 1974*a*, *Ap. J.*, **190**, 27.
———. 1974*b*, *Ap. J.*, **191**, 93.
Green, S. 1980, *Ap. J. Suppl.*, **42**, 103.
Kuiper, T. B. H., Rodríguez Kuiper, E. N., Swanson, P. N., Dickinson, D. F., Klein, M. J., and Zimmermann, P. 1984, *Ap. J.*, **283**, 106.
Kukolich, S. G. 1969, *J. Chem. Phy.*, **50**, 3751.
Kylafis, N. D., and Norman, C. 1986, *Ap. J. (Letters)*, **300**, L73.
———. 1987, *Ap. J.*, **323**, 346.

Matveenko, L. I., Graham, D. A., and Diamond, P. J. 1988, *IAU Symposium 129, The Impact of VLBI on Astrophysics and Geophysics*, ed. M. J. Reid and J. M. Moran (Dordrecht: Reidel), p. 257.
Matveenko, L. I., Kogan, L. R., and Kostenko, V. I. 1980, *Soviet Astr. (Letters)*, **6**, 279.
Matveenko, L. I., Moran, J. M., and Genzel, R. 1982, *Soviet Astr. (Letters)*, **8**(6), 382.
Matveenko, L. I., Romanov, A. M., Kogan, L. R., Moiseev, I. G., Sorochenko, R. L., and Timofeev, V. V. 1983, *Soviet Astr. (Letters)*, **9**(4), 240.
Montes, C. 1977, *Ap. J.*, **216**, 329.
Moran, J. M. 1982, *CRC Handbook of Laser Science and Technology*, Vol. **1**, *Lasers and Masers*, ed. M. J. Weber (Boca Raton, FL: CRC Press), p. 483.
Moran, J. M., *et al.* 1973, *Ap. J.*, **185**, 535.
Moran, J. M., Johnston, K. J., Spencer, J. H., and Schwartz, P. R. 1977, *Ap. J.*, **217**, 434.
Moran, J. M., Reid, M. J., Lada, C. J., Yen, J. L., Johnston, K. J., and Spencer, J. H. 1978, *Ap. J. (Letters)*, **224**, L67.
Mouschovias, T. Ch. 1976, *Ap. J.*, **207**, 141.
Myers, P. C., and Goodman, A. A. 1988, *Ap. J.*, **329**, 392.
Reid, M. J., and Moran, J. M. 1981, *Ann. Rev. Astr. Ap.*, **19**, 231.
Strelnitskii, V. S. 1980, *Soviet Astr. (Letters)*, **6**, 196.
———. 1982, *Soviet Astr. (Letters)*, **8**(2), 86.
———. 1984, *M.N.R.A.S.*, **207**, 339.
———. 1988, *IAU Symposium 129, The Impact of VLBI on Astrophysics and Geophysics*, ed. M. J. Reid and J. M. Moran (Dordrecht: Reidel), p. 239.
Sullivan, W. T. 1973, *Ap. J. Suppl.*, **25**, 393.
Tarter, J., and Welch, W. J. 1986, *Ap. J.*, **305**, 467.
Walker, R. C. 1984, *Ap. J.*, **280**, 618.
Western, L. R., and Watson, W. D. 1983, *Ap. J.*, **274**, 195.
———. 1984, *Ap. J.*, **285**, 158.
White, G. J., Avery, L. W., Richardson, K. J., and Lesurf, J. C. G. 1986, *Ap. J.*, **302**, 701.
Wynn-Williams, C. G., Genzel, R., Becklin, E. E., and Downes, D. 1984, *Ap. J.*, **281**, 172.

GUIDO GARAY: Departamento de Astronomia, Universidad de Chile, Casilla 36-D, Santiago, Chile

A. D. HASCHICK: Haystack Observatory, Off Route 40, Westford, MA 01886

J. M. MORAN: Harvard-Smithsonian Center for Astrophysics, 60 Garden Street, MS 42, Cambridge, MA 02138